Journal of The Electrochemical Society, **161** (6) A1100-A1106 (2014)
0013-4651/2014/161(6)/A1100/7/$31.00 © The Electrochemical Society

Fingerprinting Lithium-Sulfur Battery Reaction Products by X-ray Absorption Spectroscopy

Kevin H. Wujcik,[a,b,*] Juan Velasco-Velez,[c] Cheng Hao Wu,[c,d,] Tod Pascal,[e] Alexander A. Teran,[a,b] Matthew A. Marcus,[f] Jordi Cabana,[b,g,*] Jinghua Guo,[f] David Prendergast,[c] Miquel Salmeron,[c] and Nitash P. Balsara[a,b,c,*,z]**

[a]*Department of Chemical and Biomolecular Engineering, University of California, Berkeley, California 94720, USA*
[b]*Environmental Energy Technologies Division, Lawrence Berkeley National Laboratory, Berkeley, California 94720, USA*
[c]*Materials Sciences Division, Lawrence Berkeley National Laboratory, Berkeley, California 94720, USA*
[d]*Department of Chemistry, University of California, Berkeley, California 94720, USA*
[e]*Molecular Foundry, Lawrence Berkeley National Laboratory, Berkeley, California 94720, USA*
[f]*Advanced Light Source, Lawrence Berkeley National Laboratory, Berkeley, California 94720, USA*
[g]*Department of Chemistry, University of Illinois at Chicago, Chicago, Illinois 60607, USA*

Lithium-sulfur batteries have a theoretical specific energy that is a factor of five greater than that of current lithium-ion batteries, but suffer from consequences of the solubility of lithium polysulfide reaction intermediates that form as the batteries are charged and discharged. These species can react with each other and diffuse out of the cathode, causing battery capacity to fade and ultimately, cell failure. In spite of work that has spanned four decades, "fingerprints" of polysulfides have not yet been established, precluding a systematic study of lithium-sulfur chemistry. Herein we demonstrate the use of principal component analysis of X-ray absorption spectroscopy (XAS) to obtain fingerprints of lithium polysulfides. This approach enables interpretation of spectral data without any assumptions regarding the origin of the observed spectral features or knowledge of the stability of the polysulfide species of interest. We show that in poly(ethylene oxide)-based solid electrolytes containing polysulfides made by chemically reacting Li_2S and elemental sulfur, Li_2S_2 and Li_2S_6 spontaneously disproportionate to give binary Li_2S/Li_2S_4 and Li_2S_4/Li_2S_8 mixtures, respectively, while Li_2S_4 and Li_2S_8 exist as single molecular species. XAS fingerprints of Li_2S_4 and Li_2S_8 are thus presented.

Manuscript submitted March 6, 2014; revised manuscript received April 14, 2014. Published May 10, 2014. This was Paper 1234 presented at the San Francisco, California, Meeting of the Society, October 27-November 1, 2013.

Lithium-sulfur batteries have become a popular focus of energy storage research due to their high theoretical specific energy (2600 Wh/kg), which is over five times greater than current lithium-ion battery technology. Compared to active materials like cobalt oxide and iron phosphate, elemental sulfur is abundant, nontoxic and inexpensive.[1–3] The reaction mechanism through which the battery provides energy is a complex, multi-step process. The reaction scheme that is often proposed is shown in Scheme 1.

In its simplified form, the overall reduction mechanism can be written as: $S_8 + 16\,Li^+ + 16\,e^- \rightarrow 8\,Li_2S$. The intrinsic advantages of Li-S chemistry are unfortunately overshadowed by issues stemming from the fundamental properties of the Li_2S_x ($2 \leq x \leq 8$) intermediates. Due to their high solubility in common battery electrolytes, Li_2S_x species can diffuse out of the cathode during cycling and participate in a parasitic shuttle between electrodes, resulting in capacity fade and self-discharge.[4] Additionally, Li_2S_x species that diffuse to the battery anode can be irreversibly reduced to form an insulating layer of Li_2S and Li_2S_2 between the electrolyte and the negative electrode surface. These issues limit cycle life and ultimately lead to cell failure.

While a vast amount of Li-S battery research has been and is increasingly focused on solving issues related to polysulfide dissolution,[5–7] the complex reaction mechanisms through which Li_2S_x intermediates form remain unclear.[8] Sulfur reduction by lithium has been studied for over four decades, but has historically been a point of contention among researchers.[9–12] Typical approaches to examine the reaction have involved spectroelectrochemistry.[11–14] Here, electrochemical techniques (e.g. cyclic voltammetry and galvanostatic processes) are coupled with spectroscopy in an attempt to obtain spectral evidence of reaction intermediates. Spectral data obtained from these in situ experiments is interpreted by comparison to ex situ standards collected for various Li_2S_x intermediates.

Spectroelectrochemical approaches can provide powerful insight into Li-S redox pathways, as they probe chemistry in its native, unaltered environment. However, obtaining spectral fingerprints of Li_2S_x species has been problematic. Lithium polysulfide intermediates cannot be isolated,[15] and thus the fingerprints must be gathered of polysulfides dissolved in specific solvents. In solution, Li_2S_x molecules may undergo reversible disproportionation reactions to form a distribution of different Li_2S_x species via reactions (a), (b) and (c) shown in Scheme 2,[8,16] where $m \leq x - 1$ for reaction (b), and $m \geq x$ for reaction (c). Attempts to obtain standards for single Li_2S_x intermediates may instead yield spectra that represent a distribution of polysulfide molecules. It is evident from Scheme 2 that a given polysulfide

$$\text{(a)}\quad S_{8(s)} + 2\,Li^+ + 2\,e^- \rightarrow Li_2S_8$$

$$\text{(b)}\quad 3/4\,Li_2S_8 + 1/2\,Li^+ + 1/2\,e^- \rightarrow Li_2S_6$$

$$\text{(c)}\quad 2/3\,Li_2S_6 + 2/3\,Li^+ + 2/3\,e^- \rightarrow Li_2S_4$$

$$\text{(d)}\quad 1/2\,Li_2S_4 + Li^+ + e^- \rightarrow Li_2S_2$$

$$\text{(e)}\quad 1/2\,Li_2S_2 + Li^+ + e^- \rightarrow Li_2S_{(s)}$$

Scheme 1. One of many proposed schemes in the literature for the lithium-sulfur reduction pathway.

$$\text{(a)}\quad 2S_x^{2-} \leftrightarrows S_m^{2-} + \frac{x-m}{8} S_8$$

$$\text{(b)}\quad 2S_x^{2-} \leftrightarrows S_{x+m}^{2-} + S_{x-m}^{2-}$$

$$\text{(c)}\quad S_x^{2-} \leftrightarrows \frac{x-1}{m-1} S_m^{2-} + \frac{m-x}{m-1} S^{2-}$$

Scheme 2. Proposed lithium polysulfide disproportionation reactions.

*Electrochemical Society Active Member.
**Electrochemical Society Student Member.
zE-mail: nbalsara1@gmail.com

solution could contain many more than one molecular species. For example, S_6^{2-} could disproportionate to give S_4^{2-} and S_8^{2-} [reaction (b) of Scheme 2 with x = 6 and m = 2] but S_4^{2-} thus obtained may then disproportionate into other products [e.g. S_3^{2-} and S_5^{2-}; reaction (b) of Scheme 2 with x = 4 and m = 1]. Additionally, the distribution of polysulfide species present is highly dependent on the medium.[17,18] In one of the earliest UV-vis absorption spectroscopic studies of lithium polysulfides, Rauh et al. showed that spectra of lithium polysulfide solutions with identical ratios of Li:S were drastically different when THF and DMSO were solvents.[9] This was taken as a signature of different extents of disproportionation of the same lithium polysulfides in the two solvents. Obtaining unambiguous spectral fingerprints of polysulfide species has been difficult due to these issues and this has prevented researchers from reaching conclusive agreement regarding Li-S redox pathways.

X-ray absorption spectroscopy (XAS) is a well-established probe of local environment and the electronic structure of the atom of interest.[19–21] XAS in the vicinity of the sulfur K-edge is a potentially powerful technique for differentiating lithium polysulfide species. To our knowledge, XAS at the sulfur K-edge has been used to study Li-S chemistry in two previous publications. Gao et al. were the first to report XAS spectra of lithium polysulfides in battery electrolytes. However, they did not attempt to determine the relationship between measured spectra and specific polysulfide molecules that were present in the cathode.[22] More recently, Cuisinier et al. performed XAS studies of Li-S cathodes containing sulfur-imbibed spherical carbon shells.[23] They acknowledged the difficulty of interpreting measured X-ray absorption spectra due to the lack of Li_2S_x spectral standards. The determination of what polysulfide(s) spectra represent has always required auxiliary insight regarding polysulfide disproportionation.[8,16] It has not been possible to prove that the measured spectra correspond to a unique polysulfide distribution due to the complexity of reactions in Scheme 2 above.

The distinguishing feature of the present work is the use of a rigorous approach to XAS data analysis without auxiliary insight, i.e. we do not assume the presence or absence of any given polysulfide species. To do this, we employ the principal component analysis (PCA) technique as a way to determine the number of polysulfides obtained spectra represent. In previous applications to interpret XAS spectra of multicomponent systems, PCA has been used to identify different oxidation states and local environments of vanadium centers during catalytic oxidation,[24] speciate humic acid constituents in soil,[25] and elucidate the number and types of Mn-containing species in particulates emitted by gasoline engines.[26]

While previous work[23] has probed Li_2S_x species as they exist in cathodes containing liquid electrolytes, we probe Li_2S_x molecules as dilute species dissolved in solid polymer films with thicknesses below 200 nm. This combination of sulfur concentration and sample geometry is essential for obtaining spectra that are not affected by X-ray overabsorption.[27]

Experimental

Materials.— A PEO homopolymer (M_n = 50 kg/mol) sample was obtained from Polymer Source, Inc. An SEO diblock copolymer was synthesized on a high vacuum line via sequential anionic polymerization,[28] having polystyrene and poly(ethylene oxide) block molecular weights of 60 kg/mol and 63 kg/mol, respectively. Sulfur (S_8) and lithium sulfide (Li_2S) were received under argon from Alfa Aesar, opened in an argon-filled glove box, and used as received.

Lithium polysulfide solutions.— Samples for XAS experiments were prepared by spin coating thin films of SEO and PEO containing lithium polysulfide molecules onto silicon wafers (thicknesses ranging from 120–950 nm). Polysulfide/polymer/solvent solutions for spin coating were prepared by mixing Li_2S and S_8 with either PEO or SEO in either n-methylpyrrolidone (NMP) for the Li_2S_x spectra comparison study, or dimethylformamide (DMF) for the overabsorption study. DMF is more volatile than NMP, which allowed us to obtain films as thick as 950 nm by spin coating followed by drying. Solutions were mixed in sealed vials for three days at 90°C.[9] The lithium to sulfur ratio in our samples is quantified by the parameter x_{mix}. The moles of S_8 per mole of Li_2S in our systems is (x_{mix} –1)/8. If a single polysulfide species were formed by our reaction, then we would obtain:

$$Li_2S + \frac{(x_{mix} - 1)}{8} S_8 \rightarrow Li_2S_{xmix}$$

Amounts of PEO and SEO were added to each solution to obtain solution concentrations of either 50 mg polymer/mL or 100 mg polymer/mL of solvent; higher concentrations were used to obtain thicker samples. Overall sulfur concentration in polymer thin films was kept constant at 0.447 g S/g polymer for each solution. Detailed information regarding obtained x_{mix} values and sulfur concentration for each sample can be found in Table I. Calculations for the errors expressed in Table I can be found in the Supporting Information.

Table I. Experimentally obtained sulfur concentration and x_{mix} values.

Sample Name	Nominal Composition	Concentration (g S/g polymer)	x_{mix}
P2H	x_{mix} = 2, PEO	0.452 ± 0.002	1.99 ± 0.003
P4H	x_{mix} = 4, PEO	0.443 ± 0.002	4.03 ± 0.021
P6H	x_{mix} = 6, PEO	0.455 ± 0.002	6.38 ± 0.076
P8H	x_{mix} = 8, PEO	0.433 ± 0.002	8.37 ± 0.165
S2H	x_{mix} = 2, SEO	0.441 ± 0.002	2.01 ± 0.003
S4H	x_{mix} = 4, SEO	0.453 ± 0.002	4.20 ± 0.022
S6H	x_{mix} = 6, SEO	0.440 ± 0.002	5.97 ± 0.063
S8H	x_{mix} = 8, SEO	0.434 ± 0.002	8.47 ± 0.159

Solutions for x_{mix} = 2 were found to contain small amounts of precipitated solids. The reason for this will be addressed shortly. These mixtures were vigorously homogenized before solution was drawn for spin coating. There were no visible signs of precipitation in any of the other solutions (x_{mix} = 4, 6, and 8).

Polymer/polysulfide thin films.— Thin films of polysulfide-containing polymer electrolyte were obtained by spin coating onto silicon wafers. Spin coating was performed in an argon-filled glove box at room temperature. Parameters used to obtain films of different thickness ranged from 1000–4000 RPM, and 30–60 seconds of spin time. Films were allowed to dry at room temperature to prevent the sublimation of sulfur. Films were spin coated using a Chemat KW-4A spin coater. Film thickness was measured using ellipsometry (α-SE Ellipsometer, J.A. Woolman Co., Inc.).

Lithium sulfide.— In addition to the polymer film samples above, XAS measurements were also taken for Li_2S (lithium sulfide). Attempts to dissolve Li_2S in polymer/solvent were unsuccessful, and thus, samples of Li_2S for XAS consisted of pure Li_2S powder. This powder was lightly dusted onto sulfur-free tape and measured in fluorescence mode.

X-ray absorption spectroscopy.— X-ray absorption spectra were obtained at beamline 4–3 of the Stanford Synchrotron Radiation Lightsource (SSRL) and were taken in fluorescence mode using a 4-element silicon Vortex detector. Energy calibration was carried out using thiosulfate, setting the first peak centroid to 2472.02 eV. Spectra were taken for a range of 2440 to 2575 eV with an energy resolution as low as 0.08 eV near the absorption edge. Three consecutive scans were taken for each sample without any movement of the sample stage between scans and then averaged for further data analysis. No differences were observed between consecutive scans. X-ray spectra were normalized and background subtracted using SIXPACK.[29]

To prevent the exposure of samples to air, samples were transferred from the glove box at Lawrence Berkeley National Laboratory (LBNL) in an argon-filled desiccator to the Stanford Synchrotron Radiation Lightsource (SSRL) where they were placed in an

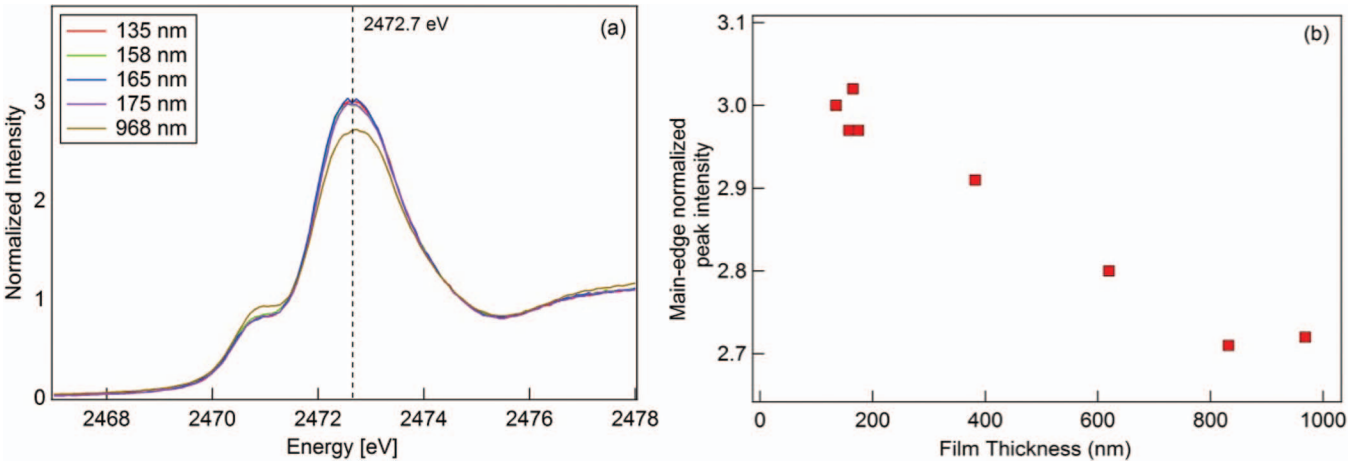

Figure 1. (a) XAS spectra in the vicinity of the sulfur K-edge of thin films of $x_{mix} = 8$ samples in PEO with different film thicknesses. (b) Main-edge peak intensity as a function of film thickness; the decrease in intensity is due to X-ray overabsorption.

argon-filled glove box. Samples were transferred from the glove box to the beamline endstation via an air-tight container and loaded into the helium-filled measurement chamber through a helium-filled glove-bag equipped with an oxygen sensor. The effect that air-exposure has on obtained spectra was examined as shown in the Supporting Information.

X-ray overabsorption.— Interpretation of XAS spectra is simplified in the absence of overabsorption (sometimes referred to as self-absorption in the literature), a phenomenon that occurs for samples that are too thick or too concentrated.[30–32] Spectra affected by overabsorption tend to display dampened spectral features with strong relative absorption and, hence, enhanced spectral features with weak relative absorption. This would likely lead to spurious relative intensities between observed pre- and main-edge features in our S K-edge, and, as we will show, these two spectral features are critical for determining the distribution of polysulfide species in samples. To elucidate the effect of overabsorption on Li_2S_x spectra, thin films of PEO containing $x_{mix} = 8$ were spun cast to obtain a range of thicknesses; sulfur K-edge spectra were obtained for each thickness. In Figure 1a we show XAS spectra at selected film thicknesses. The intensity of the main-edge peak occurring at 2472.7 eV is plotted as a function of film thickness in Figure 1b. The main-edge peak intensity is 2.98 ± 0.02 when film thickness is less than 200 nm. In contrast, the main-edge peak intensity of films with thickness greater than 200 nm is significantly lower, reaching a value of about 2.71 as film thickness exceeded 900 nm. The XAS spectra of samples with thicknesses between 135 and 175 nm were almost indistinguishable from each other (see Figure 1a). Thus, to mitigate the effects of overabsorption, the samples used to obtain spectra shown throughout the remainder of this work were all cast to be between 120 and 180 nm.

The effect of overabsorption is also dependent on the overall concentration of sulfur atoms in a sample. For this reason, all samples contained an equivalent overall sulfur concentration of 0.447 g S/ g polymer. No mathematical corrections for overabsorption were performed on the data presented here.

Principal component analysis.— The PCA was performed using algorithms described by Ressler.[26] In brief, PCA works by reducing the dimensionality of the X-ray spectra dataset by finding independent components that, through linear combination, can be used to simulate experimental data within statistical significance.[33–36]

Discussion

We begin our analysis by examining sulfur K-edge XAS data collected for polysulfide-containing polymer electrolyte thin films. Figure 2a, 2b show the normalized sulfur K-edge spectra collected for samples having x_{mix} values of 2, 4, 6, and 8 dissolved in solid thin films of PEO and SEO at a constant sulfur concentration of 0.447 g S / g polymer. Spectra obtained from SEO and PEO mixtures for a given value of x_{mix} are nearly indistinguishable (Figures 2a and 2b). Also shown is the XAS spectrum for pure Li_2S powder (Figure 2c).

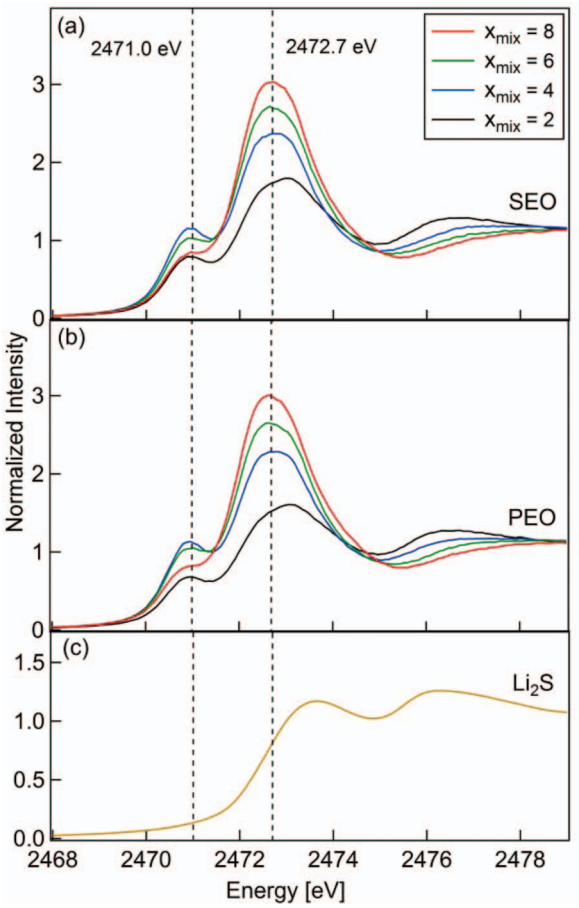

Figure 2. Experimentally measured sulfur K-edge XAS spectra of Li_2S_{xmix} in polymer thin film samples (thicknesses less than 180 nm) in (a) SEO and (b) PEO at a sulfur concentration of 0.447 g S/g polymer, and (c) pure Li_2S powder lightly dusted onto sulfur-free tape.

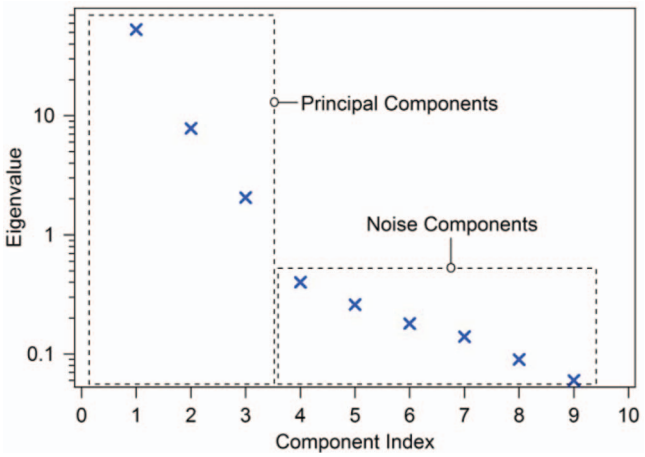

Figure 3. Scree plot of principal component analysis eigenvalues.

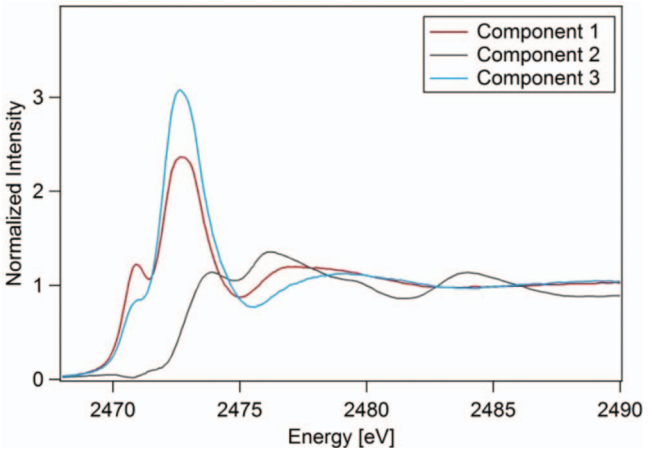

Figure 4. X-ray absorption spectra of principal components obtained from analysis of the full XAS data set. Components 1, 2, and 3 are identified as Li_2S_4, Li_2S and Li_2S_8, respectively, based on the parsimonious interpretation of the full XAS data set.

The energy range over which XAS data are obtained in this study (Figure 2) are in close proximity to the sulfur K-edge. It is well known that data obtained in this regime, often referred to as X-ray absorption near-edge structure (XANES) spectra, are similar to other forms of absorption spectra known in chemistry, wherein the measured signal reflects the molecular species present in solution. Given that XAS is a bulk spectroscopic technique, the resulting XANES region is due to the weighted average of the XANES of all molecular species present in the sample. If reference spectra for known species are available, then linear least-squares fitting may be used to measure the fractions of each species represented by each spectrum. While we have obtained a reference spectrum for Li_2S, no such spectra exist for Li_2S_x species ($2 \leq x \leq 8$). We must use statistical methods to interpret the data shown in Figure 2. PCA seeks to describe the set of spectra as weighted sums of a smaller number of "component" spectra, the relative importance of which is measured by the "eigenvalue" of each component. Semi-empirical methods exist to determine the minimum number of components required to describe a given dataset.[34] Results of the application of PCA to the dataset of nine experimental spectra (Li_2S_{xmix} in PEO & SEO, and Li_2S) are shown in Figure 3, where components are rank-ordered according to the magnitude of their corresponding eigenvalue (also known as a scree plot).[33] Note that our analysis is restricted to four different x_{mix} compositions: $x_{mix} = 2, 4, 6, 8$ in PEO & SEO. On a semi-log plot, there is a kink which separates the first three components from the rest, suggesting that the systems of interest contain three underlying components. These are our principal components. Reconstruction of the data using these three components shows satisfactory agreement with the original spectra.

Another approach for distinguishing between noise and principal components was proposed by Malinowski, who suggests calculating the value indicator function (IND).[34] The values of IND obtained for each component are shown in Table II along with their eigenvalue. The distinction between principal and noise components is predicted to occur at the component index where IND is a minimum. As seen in Table II, this occurs for the component index of three. It is thus evident both from the scree plot and the IND analysis that the XAS spectra from our collection of samples contain three principal components.

Table II. Principal component eigenvalues and IND values.

Principal Component	Eigenvalue	IND values
1	53.0	4.47e-2
2	7.81	1.63e-2
3	2.05	6.11e-3
4	0.40	6.47e-3
5	0.26	7.76e-3
6	0.18	1.13e-2
7	0.14	1.88e-2
8	0.09	6.08e-2
9	0.06	-

The abstract component spectra generated by the PCA procedure contain unphysical features (e.g. negative aborption values in the energy range of interest). The standard procedure to obtain X-ray spectra that do not contain such unphysical features is the iterative transformation factor analysis (ITFA) as described in reference.[37] In this step of the analysis, one constructs new "components" from weighted sums of the abstract components in such a way that the amounts of each ITFA component required to fit all spectra are between 0 and 1 and as different from each other as possible. This method has been shown to result in ITFA spectra which often represent molecular species or combinations of a small number of molecular species. ITFA was applied to the results of the PCA and the computed spectrum of principal components one, two and three are shown in Figure 4. The weightings of each computed spectrum needed to recreate the experimentally measured spectra for all our samples were calculated and the results are plotted on a ternary composition diagram in Figure 5a.

Each corner of the ternary diagram represents the spectrum of one of the principal components shown in Figure 4, and binary mixtures of components are located along the sides of the triangle. The bracketed numbers near the corners of the ternary composition diagram in Figure 5 represent the specific components identified in Figure 4. It is remarkable that all of our samples are located either near the corners or the sides of the ternary diagram. This indicates that our samples are, to a good approximation, either single component or two component mixtures. It is evident in Figure 5a that Li_2S is located very close to the corner corresponding to component 2. We know for a fact that our Li_2S sample is a pure component. We thus expect the PCA to interpret the Li_2S data as such. The fact that the Li_2S data point in Figure 5a is not exactly at the apex of the triangle may be due to noise in the data and limitations of the PCA approach. Recognizing this, we still assert that component 2 is Li_2S. Note the similarity between the XAS spectrum of component 2 obtained by the PCA (Figure 4) and the measured spectrum of Li_2S (Figure 2c).

The bottom left corner of the triangle in Figure 5a represents principal component 1 and the bottom right, principal component 3. Samples of $x_{mix} = 4$ are located near the bottom left corner of the diagram, while $x_{mix} = 8$ are located near the bottom right corner. The parsimonious interpretation of these observations is that principal component 1 is Li_2S_4 and principal component 3, Li_2S_8. The component corners in Figure 5a are thus labeled Li_2S (p), Li_2S_4 (p) and Li_2S_8 (p), where '(p)' denotes the fact that these assignments originate from the PCA. We have thus established a correspondence

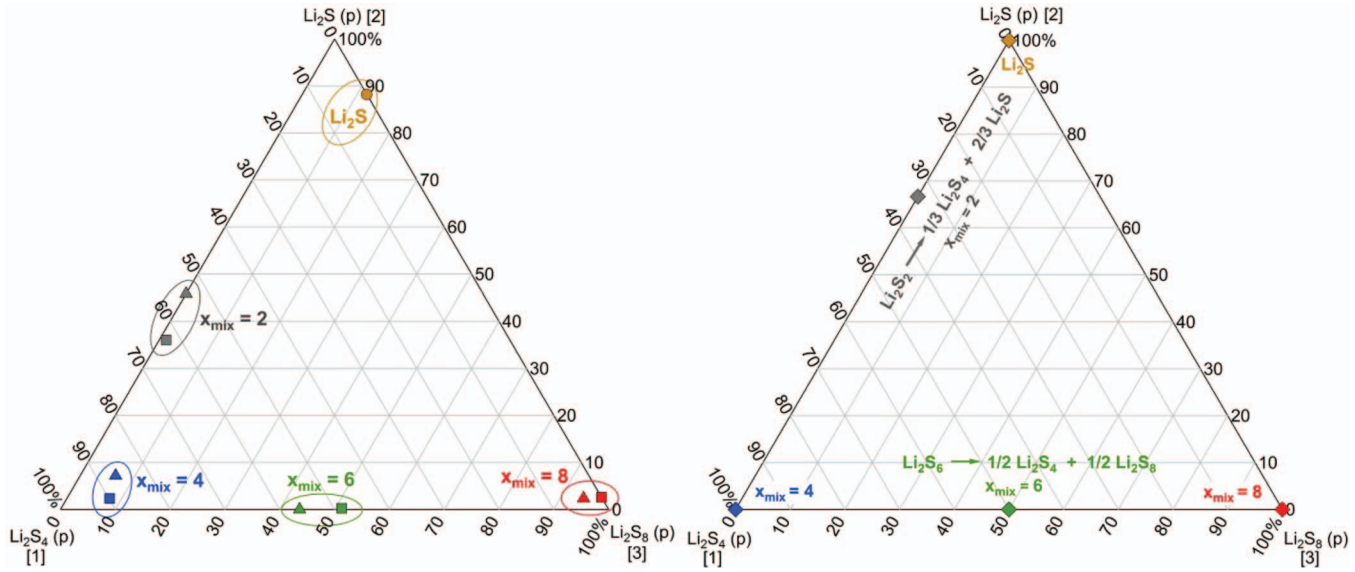

Figure 5. (a) Compositions of Li_2S_{xmix} and Li_2S samples plotted on a ternary diagram, determined by principal component analysis of the full XAS data set. Samples that lie near the corners are, to a good approximation, one-component systems. Samples that lie near the sides of the triangle but away from the corners are, to a good approximation, two-component systems. Squares and triangles represent polysulfides dissolved in SEO and PEO, respectively. (b) Theoretical ternary composition diagram of Li_2S_{xmix} and Li_2S samples if only the $x_{mix} = 2$ and $x_{mix} = 6$ samples participated in disproportionation reactions as shown. Qualitative agreement between the experimental and theoretical ternary composition diagrams supports the proposed disproportionation scheme (see text for details).

between the abstract *components* determined by PCA and molecular *species*.

Figure 5a shows that the $x_{mix} = 2$ samples are, to a good approximation, binary mixtures of Li_2S_4 and Li_2S. It is thus evident that Li_2S_2 species do not exist in the $x_{mix} = 2$ mixtures. Specifically, Li_2S_2 disproportionates into Li_2S and Li_2S_4. The fact that the $x_{mix} = 2$ data lie on the Li_2S—Li_2S_4 side of the triangle in Figure 5a indicates the absence of Li_2S_8. The expected disproportionation reaction is then:

$$Li_2S_2 \rightleftarrows 1/3\,Li_2S_4 + 2/3\,Li_2S$$

This corresponds to disproportionation reaction 'c' in Scheme 2 given in the introduction with $x = 2$ and $m = 4$. Note that the proposed equilibrium is dominated by the forward reaction. Since Li_2S is an insoluble solid, our observation of precipitates in $x_{mix} = 2$ solutions (see Experimental section) is likely to be due to its presence.

Similarly, Figure 5a shows that $x_{mix} = 6$ samples are binary mixtures of Li_2S_4 and Li_2S_8. The expected disproportionation reaction is:

$$Li_2S_6 \rightleftarrows 1/2\,Li_2S_4 + 1/2\,Li_2S_8$$

This corresponds to disproportionation reaction 'b' in Scheme 2 given in the introduction with $x = 6$ and $m = 2$. Note that the proposed equilibrium is dominated by the forward reaction.

Figure 5b shows the expected locations of $x_{mix} = 2, 4, 6, 8$ and Li_2S samples in the case that: (a) $x_{mix} = 4$, $x_{mix} = 8$, and Li_2S experimental spectra were identical to the generated principal components, and (b) the experimental spectra for $x_{mix} = 2$ and 6 represented the complete disproportionation reactions proposed above without any error. One might consider Figure 5b to be the ideal ternary diagram representing the parsimonious interpretation of the PCA results. The observed differences between the location of data points in Figures 5a and 5b are probably due to noise in the data or inherent uncertainties in component spectra determined by PCA. The qualitative similarity between the measured and ideal ternary diagrams is noteworthy, particularly when one considers the fact that the PCA analysis is not constrained to any particular stoichiometry.

To further explore the robustness of the conclusion regarding Li_2S_6 disproportionation to form Li_2S_4 and Li_2S_8, we calculated a 50/50 weighted sum of the experimental spectra of $x_{mix} = 4$ and $x_{mix} = 8$ PEO samples. This calculated spectrum is compared to the experimental spectrum obtained from the $x_{mix} = 6$ PEO in Figure 6a. The absolute value of the difference between the experimental and calculated spectra intensity shown in Figure 6b is relatively small. This comparison mainly serves to show the internal consistency of our PCA-based conclusion regarding the disproportionation of Li_2S_6 (Scheme 2, reaction (b)) to form Li_2S_4 and Li_2S_8.

We then aimed to test whether the calculation described in the previous paragraph would hold for other spectra where we concluded that disproportionation did not take place. In other words, is it possible to represent any x_{mix} spectrum as a combination of $(x_{mix} - 2)$ and $(x_{mix} + 2)$ spectra? Such a calculation was performed for the $x_{mix} = 4$ sample to determine if the $x_{mix} = 4$ spectrum could be represented by equal parts $x_{mix} = 2$ and $x_{mix} = 6$, corresponding to a hypothetical disproportionation reaction: $2\,Li_2S_4 \rightarrow Li_2S_6 + Li_2S_2$ (according to Scheme 2, reaction (b)). The results of this calculation are shown in Figures 6c and 6d. The difference between the experimental and calculated spectra obtained for this hypothetical reaction shown in Figure 6d is significantly larger than that for Li_2S_6 disproportionation by Scheme 2, reaction (b) as shown in Figure 6b. This indicates that the hypothetical reaction ($2\,Li_2S_4 \rightarrow Li_2S_6 + Li_2S_2$) proposed in this paragraph is inconsistent with our data. The results in Figure 6 support the conclusion that that Li_2S_6 disproportionates to form Li_2S_4 and Li_2S_8.

The disproportionation reaction we propose here is different from those reported by Cuisiner et al. who studied sulfur cathodes with a mixture of 1,3-dioxolane, 1,2- dimethoxyethane, $LiClO_4$, and $LiNO_3$ as the electrolyte.[23] They concluded that Li_2S_6 does not disproportionate, while Li_2S_8 does. The difference between our conclusions and those reported by Cuisiner et al. may be due to the differences in the systems examined. In particular, our work studies polysulfides in polymer electrolytes with no added salt while Cuisiner et al. studied polysulfides generated via redox reaction in the cathode in the presence of $LiClO_4$ and $LiNO_3$. Additionally, the polysulfide species of this work were obtained by chemical reactions, rather than electrochemical reactions.

While the above analysis has focused on the parsimonious interpretation of the XAS data based on PCA, it is not unique. For example, if a constant fraction of a fourth species were present in all samples, PCA would still indicate three principal components, but the

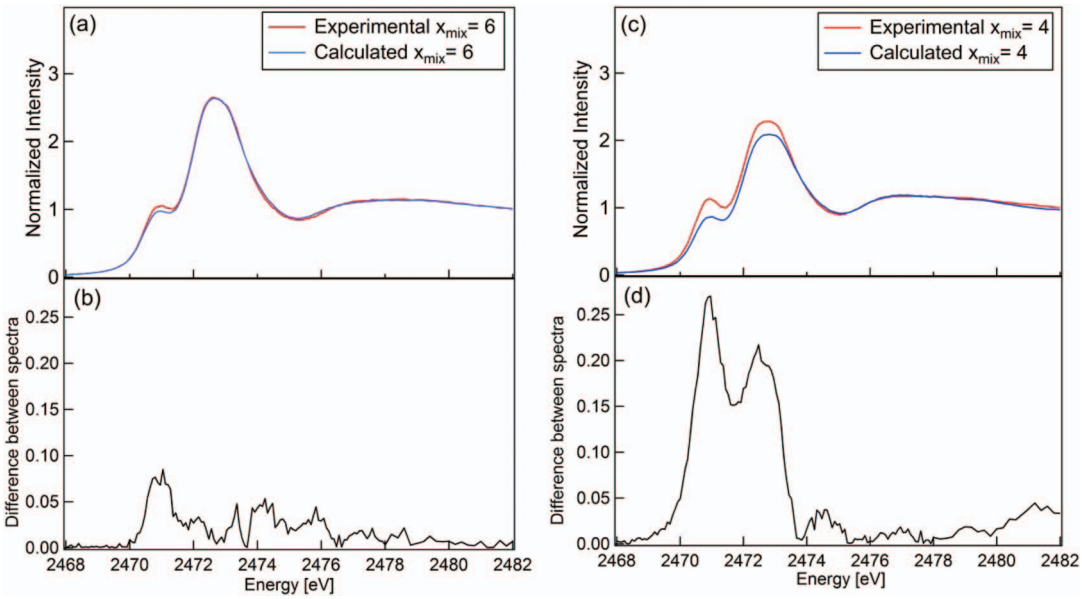

Figure 6. (a) XAS spectra of an Li_2S_{xmix} sample in PEO with $x_{mix} = 6$: Calculated using a weighted sum of spectra obtained from $x_{mix} = 4$ and $x_{mix} = 8$ samples, and one obtained directly by experiment. (b) Absolute value of the difference between experimental and calculated spectra in (a). (c) XAS spectra of an Li_2S_{xmix} sample with $x_{mix} = 4$: Calculated using a weighted sum of spectra obtained from $x_{mix} = 2$ and $x_{mix} = 6$ samples, and one obtained directly by experiment. (d) Absolute value of the difference between experimental and calculated spectra in (c). The small difference in (b) supports disproportionation in Li_2S_{xmix} sample with $x_{mix} = 6$, while the large difference in (d) indicates that the data do not support disproportionation in Li_2S_{xmix} sample with $x_{mix} = 4$.

component spectra thus generated would not represent single molecular species. Note that this is highly unlikely as reactions involving polysulfides must be consistent with strict stoichiometric constraints (e.g. Scheme 2). Nevertheless, further work is needed to critically evaluate the validity of the proposed disproportionation schemes.

Conclusions

Solid-state polymer films of PEO and SEO containing Li_2S_x molecules as well as Li_2S powder were examined using XAS at the sulfur K-edge. Principal component analysis was performed on the system of collected X-ray spectra to obtain spectral fingerprints of individual polysulfide species. The present approach to spectral data interpretation makes no assumption regarding polysulfide disproportionation. We believe the coupling of XAS with PCA will stand as an effective tool for spectroelectrochemical studies of Li-S battery reaction mechanisms.

Our analysis revealed that spectra obtained at all x_{mix} values (2, 4, 6, 8) could be represented as mixtures of one or two principal components. The PCA results were quantified on a ternary diagram (Figure 5a). The data for Li_2S and $x_{mix} = 4$ and 8 samples were located close to the corners of the ternary diagram. Our parsimonious interpretation is that the $x_{mix} = 4$ and 8 samples were composed of nearly pure molecular species, Li_2S_4 and Li_2S_8, respectively. In contrast samples of $x_{mix} = 2$ and 6 were located on the binary mixture lines. The fact that the most complex polysulfide containing mixtures in PEO-based electrolytes have only two components is a remarkable simplification. The location of $x_{mix} = 2$ samples suggests that Li_2S_2 disproportionates to form the Li_2S_4 and Li_2S, while the location of $x_{mix} = 6$ data suggests that Li_2S_6 disproportionates to form Li_2S_4, and Li_2S_8. The implication of these results is that complex reaction pathways similar to the proposed example shown in Scheme 1 would be highly simplified. Essentially, steps (b) and (d) would be skipped over, as Li_2S_6 and Li_2S_2 disproprotionate spontaneously to give Li_2S_8 and Li_2S_4, and Li_2S and Li_2S_4, respectively. Further work is needed to determine the kinetics of disproportionation. If this simplification is also valid in polysulfides created by electrochemical driving forces in the lithium-sulfur battery, then resolving issues related to capacity fading may be addressed by focusing on the containment of only two species: Li_2S_4 and Li_2S_8.

Note that no knowledge of the relationship between observed peaks in the XAS spectra and specific electronic transitions of particular species was used to determine polysulfide disproportionation. In future work we will use molecular simulations and other complimentary experimental tools to critically examine the conclusions made in this study. In particular, we plan to study the products of electrochemical reduction of sulfur in appropriately designed in situ XAS cells. The species that are created in electrochemical cells may be different from those detected in the present work, which is limited to chemically synthesized polysulfides.

Acknowledgments

We acknowledge the help of Erik Nelson and Matthew Latimer of SSRL beamline 4–3, and Wayne Stolte of the Advanced Light Source (ALS) beamline 9.3.1, where preliminary work was performed. Preliminary work was also performed at ALS beamline 10.3.2. The authors acknowledge Rachel Segalman for use of ellipsometry equipment, and Mukes Kapilishrami for valuable advice regarding the XAS experiments. J. Velasco-Velez gratefully acknowledges financial support from the Alexander von Humboldt foundation.

This work was supported by the Assistant Secretary for Energy Efficiency and Renewable Energy, Office of Vehicle Technologies of the U.S. Department of Energy under Contract DE-AC02–05CH11231 under the Batteries for Advanced Transportation Technologies (BATT) Program.

Portions of this research were carried out at the Stanford Synchrotron Radiation Lightsource, a Directorate of SLAC National Accelerator Laboratory and an Office of Science User Facility operated for the U.S. Department of Energy Office of Science by Stanford University. The SSRL Structural Molecular Biology Program is supported by the DOE Office of Biological and Environmental Research, and by the National Institutes of Health, National Institute of General Medical Sciences (including P41GM103393). The contents of this publication are solely the responsibility of the authors and do not necessarily represent the official views of NIGMS or NIH.

Complimentary XAS experiments were also conducted at the Advanced Light Source, supported by the Director, Office of Science, Office of Basic Energy Sciences, of the U.S. Department of Energy under Contract No. DE-AC02–05CH11231.

List of Symbols

Abbreviations	
DMF	dimethylformamide
IND	indicator function
ITFA	iterative transformation factor analysis
Li-S	Lithium-sulfur
NMP	n-methylpyrrolidone
PCA	principal component analysis
PEO	poly(ethylene oxide)
SEO	polystyrene-poly(ethylene oxide)
SIXPACK	Sam's Interface for XAS analysis Package
THF	tetrahydrofuran
XAS	x-ray absorption spectroscopy

References

1. R. D. Rauh, K. M. Abraham, G. F. Pearson, J. K. Surprenant, and S. B. Brummer, *Journal of The Electrochemical Society*, **126**, 523 (1979).
2. V. S. Kolosnitsyn and E. V. Karaseva, *Russ J Electrochem*, **44**, 506 (2008).
3. S. B. R. Brummer, R. D. Marston, and J. M. Shuker, R. S. Low Temperature Lithium/Sulfur Secondary Battery, in, p. 1, Research and Development Administration, US Department of Energy, Washington, DC (1976).
4. Y. V. Mikhaylik and J. R. Akridge, *Journal of The Electrochemical Society*, **151**, A1969 (2004).
5. X. Ji, K. T. Lee, and L. F. Nazar, *Nature Materials*, **8**, 500 (2009).
6. H. Wang, Y. Yang, Y. Liang, J. T. Robinson, Y. Li, A. Jackson, Y. Cui, and H. Dai, *Nano Letters*, **11**, 2644 (2011).
7. C. Liang, N. J. Dudney, and J. Y. Howe, *Chemistry of Materials*, **21**, 4724 (2009).
8. C. Barchasz, F. Molton, C. Duboc, J. C. Lepretre, S. Patoux, and F. Alloin, *Analytical Chemistry*, **84**, 3973 (2012).
9. R. D. Rauh, F. S. Shuker, J. M. Marston, and S. B. Brummer, *Journal of Inorganic and Nuclear Chemistry*, **39**, 1761 (1977).
10. H. Yamin, J. Penciner, A. Gorenshtain, M. Elam, and E. Peled, *Journal of Power Sources*, **14**, 129 (1985).
11. B. S. Kim and S. M. Park, *Journal of The Electrochemical Society*, **140**, 115 (1993).
12. D.-H. Han, B.-S. Kim, S.-J. Choi, Y. Jung, J. Kwak, and S.-M. Park, *Journal of The Electrochemical Society*, **151**, E283 (2004).
13. Y. Diao, K. Xie, S. Xiong, and X. Hong, *Journal of The Electrochemical Society*, **159**, A1816 (2012).
14. M. Hagen, P. Schiffels, M. Hammer, S. Dörfler, J. Tübke, M. J. Hoffmann, H. Althues, and S. Kaskel, *Journal of The Electrochemical Society*, **160**, A1205 (2013).
15. T. T. Pickering, A., *Sulfur in Organic and Inorganic Chemistry*, New York (1972).
16. A. Kamyshny, A. Goifman, J. Gun, D. Rizkov, and O. Lev, *Environmental Science and Technology*, **38**, 6633 (2004).
17. F. Gaillard and E. Levillain, *Journal of Electroanalytical Chemistry*, **398**, 77 (1995).
18. R. P. Martin, W. H. Doub, J. L. Roberts, and D. T. Sawyer, *Inorganic Chemistry*, **12**, 1921 (1973).
19. P. Eisenberger and B. M. Kincaid, *Science*, **200**, 1441 (1978).
20. D. E. Sayers, E. A. Stern, and F. W. Lytle, *Physical Review Letters*, **27**, 1204 (1971).
21. J. Yano and V. K. Yachandra, *Photosynthesis research*, **102**, 241 (2009).
22. J. Gao, M. A. Lowe, Y. Kiya, and H. D. Abruña, *The Journal of Physical Chemistry C*, **115**, 25132 (2011).
23. M. Cuisinier, P.-E. Cabelguen, S. Evers, G. He, M. Kolbeck, A. Garsuch, T. Bolin, M. Balasubramanian, and L. F. Nazar, *The Journal of Physical Chemistry Letters*, **4**, 3227 (2013).
24. M. Ruitenbeek, A. J. van Dillen, F. M. F. de Groot, I. E. Wachs, J. W. Geus, and D. C. Koningsberger, *Topics in Catalysis*, **10**, 241 (2000).
25. S. Beauchemin, D. Hesterberg, and M. Beauchemin, *Soil Science Society of America Journal*, **66**, 83 (2002).
26. T. Ressler, J. Wong, J. Roos, and I. L. Smith, *Environmental Science and Technology*, **34**, 950 (2000).
27. J. Goulon, C. Goulon-Ginet, R. Cortes, and J. M. Dubois, *Journal De Physique*, **43**, 539 (1982).
28. M. Singh, O. Odusanya, G. M. Wilmes, H. B. Eitouni, E. D. Gomez, A. J. Patel, V. L. Chen, M. J. Park, P. Fragouli, H. Iatrou, N. Hadjichristidis, D. Cookson, and N. P. Balsara, *Macromolecules*, **40**, 4578 (2007).
29. S. M. Webb, *Physica Scripta*, **2005**, 1011 (2005).
30. A. Manceau and K. L. Nagy, *Geochimica et Cosmochimica Acta*, **99**, 206 (2012).
31. I. J. Pickering, G. N. George, E. Y. Yu, D. C. Brune, C. Tuschak, J. Overmann, J. T. Beatty, and R. C. Prince, *Biochemistry*, **40**, 8138 (2001).
32. L. Tröger, D. Arvanitis, K. Baberschke, H. Michaelis, U. Grimm, and E. Zschech, *Physical Review B*, **46**, 3283 (1992).
33. F. I. Allen, M. Watanabe, Z. Lee, N. P. Balsara, and A. M. Minor, *Ultramicroscopy*, **111**, 239 (2011).
34. E. R. Malinowski, *Factor Analysis in Chemistry*, John Wiley & Songs, Inc., New York (1991).
35. A. I. Frenkel, O. Kleifeld, S. R. Wasserman, and I. Sagi, *Journal of Chemical Physics*, **116**, 9449 (2002).
36. S. R. Wasserman, P. G. Allen, D. K. Shuh, J. J. Bucher, and N. M. Edelstein, *Journal of Synchrotron Radiation*, **6**, 284 (1999).
37. A. C. Scheinost, A. Rossberg, M. Marcus, S. Pfister, and R. Kretzschmar, *Physica Scripta*, **2005**, 1038 (2005).